Effect of emission variability on concentration fluctuations in idealised deep urban street canyons

Urban Climate 55 (2024) 101952

Contents lists available at ScienceDirect

Urban Climate

journal homepage: www.elsevier.com/locate/uclim

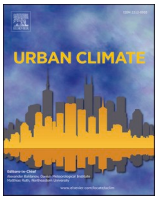

# Effect of emission variability on concentration fluctuations in idealised deep urban street canyons

Sofia Fellini [a,*], Pietro Salizzoni [b], Luca Ridolfi [a]

[a] Department of Environmental, Land and Infrastructure Engineering, Politecnico di Torino, Turin 10129, Italy
[b] Laboratoire de Mécanique des Fluides et d'Acoustique, UMR CNRS 5509, Université de Lyon, École Centrale de Lyon, INSA Lyon, Université Claude Bernard Lyon I, Écully 69134, France

ARTICLE INFO

*Keywords:*
Urban air quality
Street canyon
Emission variability
Dynamical systems
Two-box model
Stochastic analysis

ABSTRACT

The level of air pollution in a street canyon depends on the non-trivial interplay between vehicular exhaust emissions, atmospheric transport, and physico-chemical transformation of pollutants. In this study, we investigate the temporal dynamics of air pollutant concentration in a deep street canyon orthogonal to the wind direction using a two-box model. Simulations provide insights into both steady-state mean concentrations and the magnitude of concentration fluctuations as pollutant nature (inert or reactive), emission signal stochasticity, and the fundamental rates of turbulent transport and chemical transformations vary. Beyond elucidating the role of different parameters on mean pollution levels, the results reveal that extreme air pollutant concentrations are more likely to occur when the characteristic time scale of vehicular exhaust emissions significantly exceeds the ventilation time scale of the street canyon. The innovative modelling approach paves the way for various applications, particularly in the field of optimal traffic management and the study of citizens' exposure to air pollution.

## 1. Introduction

Nowadays, urban areas face significant challenges related to the urban microclimate and especially to air pollution. According to the latest WHO (World Health Organization) report (WHO, 2023), almost all of the global population (99%) breathe air that exceeds WHO guideline limits. This is responsible for around 7 million premature deaths per year (Murray et al., 2020). The vulnerability of cities to air pollution is due, on one hand, to the high number and magnitude of polluting emissions in densely populated areas and, on the other hand, to the intricate urban geometry that limits ventilation (Li et al., 2021; Fellini et al., 2020b, 2021). In urban street canyons, turbulent transport is inhibited and the wind-induced flow field depends on several factors such as the geometry of the canyon (e.g., Jeong and Andrews, 2002; Xiaomin et al., 2006), its orientation with respect to the wind (Soulhac et al., 2008), the presence of obstacles such as trees (Gromke and Ruck, 2012; Fellini et al., 2022; Carlo et al., 2023; Del Ponte et al., 2024), and thermal effects that induce buoyancy flows (Marucci and Carpentieri, 2019; Fellini et al., 2020a). Typically, the attention is directed towards street canyons oriented perpendicular to the wind direction, as this configuration exhibits the highest air pollutant concentrations. This is primarily attributed to the formation of one or multiple recirculating vortices within the canyon, as numerically and experimentally evidenced in previous literature (e.g., Sini et al., 1996; Lee and Park, 1994; Jeong and Andrews, 2002; Assimakopoulos et al., 2003; Louka et al., 2002; Liu et al., 2004; Allegrini et al., 2013; Marucci and Carpentieri, 2019; Fellini et al., 2020a). These recirculating

* Corresponding author.
*E-mail address:* sofia.fellini@polito.it (S. Fellini).

https://doi.org/10.1016/j.uclim.2024.101952
Received 24 August 2023; Received in revised form 10 April 2024; Accepted 24 April 2024
Available online 7 May 2024

structures restrict the transport of pollutants and confines them at street level, where they are emitted.

Vehicular traffic stands out as the predominant source responsible for surpassing air quality standards in city centres (EEA, 2021). The combustion processes by motor vehicles are mainly responsible for the emissions of nitrogen oxides ($NO_x$) which, upon acute exposure, can lead to respiratory ailments and impair lung function. Children are particularly susceptible, as evidenced by an elevated occurrence of childhood asthma attributed to $NO_x$ emissions from vehicular traffic (Khreis et al., 2017; Anenberg et al., 2022). The repartition of $NO_x$ at the emission is approximately between 10% to 15% for nitrogen dioxide ($NO_2$) and, thus, 90% to 85% for nitrogen monoxide (NO) (Ntziachristos et al., 2000). While NO is the primary contributor to $NO_x$, it is less toxic than $NO_2$. However, due to its inherent instability as a radical, NO readily undergoes photochemical oxidation to form $NO_2$. Nitrogen dioxide can subsequently undergo photolysis, converting back to NO and leading to the generation of ozone ($O_3$) (Oke et al., 2017). These chemical transformations can be succinctly represented by a minimalistic 3-reaction scheme involving $NO_2$-NO-$O_3$ (Soulhac et al., 2011). However, a more comprehensive depiction encompasses the intricate interactions involving radicals resulting from the oxidation of volatile organic compounds (VOC) and carbon monoxide (CO) (Jenkin and Clemitshaw, 2000), as well as interactions with hydroxyl radicals, ultimately leading to the production of nitric acid.

The fate of pollutants emitted at street level relies thus on both complex chemical transformations as well as transport dynamics governed by the turbulent flow. Previous studies have shown that, within busy street canyons, chemical reactions occur on a timescale similar to that of canyon air circulation and residence time of pollutants (Soulhac et al., 2023). Therefore, it is crucial to model both dynamics (chemical and turbulent) in order to accurately simulate air pollutant concentrations.

Extensive research has been conducted over the past two decades to investigate the interplay between turbulent and chemical dynamics in assessing photochemical pollution in urban areas, as reviewed by Zhong et al. (2016a). Especially, Computational Fluid Dynamics (CFD) has played a key role in providing insights into this domain (e.g., Garmory et al., 2009; Kwak and Baik, 2012; Kim et al., 2012). By means of CFD simulations, both the turbulent flow field and the chemical reactions can be reproduced with great accuracy. Nevertheless, the range of scenarios to be simulated in an urban environment is extensive, given the diverse street geometries, meteorological conditions, and emission modes. Since the domain and model configurations should be tailored on a case-by-case basis, employing CFD models for such a wide range of scenarios is computationally demanding and resource-intensive. For these reasons, a more efficient way is adopting simplified modelling approaches as box models (Vardoulakis et al., 2007).

Box models partition a street canyon into one or several regions (referred to as boxes), with each box associated with a mass balance equation. One-box models for non-reactive pollutants have been widely studied (Berkowicz, 2000; Soulhac, 2000; Kukkonen et al., 2001; Caton et al., 2003). However, both experimental observations and numerical simulations have shown that air pollutant concentration is far from being spatially uniform in street canyons (e.g., Assimakopoulos et al., 2003; Marucci and Carpentieri, 2019), and more than one time scale is involved in the ventilation process (Salizzoni et al., 2009; Fellini et al., 2020a). Therefore, a comprehensive understanding of the wash-out process requires the adoption of multi-box models (Salizzoni et al., 2009; Murena et al., 2011). Regarding chemical transformations, photochemical smog has been incorporated into a one-box chemistry model by Liu and Leung (2008) and into a two-box model by Zhong et al. (2015) and Zhong et al. (2016b). Furthermore, the investigation conducted by Soulhac et al. (1) validated the outcomes of a box model employing the simplified NO-$NO_2$-$O_3$ cycle through field measurements conducted in three urban canyons in the city of Lyon (France).

Historically, box models have predominantly been employed to assess steady-state air pollutant concentrations within street canyons, offering valuable approximations for operational models at the urban scale (Carruthers et al., 2000; Soulhac et al., 2011). Nevertheless, these models can also be effectively employed to delve into transient behaviors and investigate the influence of diverse parameters on the system's dynamics. Such analyses become particularly intriguing when the system's external forces exhibit temporal variability, as is often the case with vehicular emissions.

The passage of a single car, traffic flow regulated by traffic lights, or daily traffic patterns are characterized by a temporal scale that can range from seconds to hours. The variability in emission rates over time significantly influences concentration trends and, consequently, the levels of pollution to which residents are exposed. Moreover, the presence of chemical reactions introduces non-linear behaviors that can further amplify traffic-induced variations in pollutant concentrations. The evaluation of peak concentration values is crucial as short-term exposure to high peaks is associated with respiratory and cardiovascular health issues (Cassiani et al., 2020).

In this framework, the objective of this study is to adopt a box model for a street canyon with either inert or reactive pollutant emissions to evaluate how the typical time scales of canyon ventilation and chemistry interact with the time scale of traffic emissions at the street level. The study aims to analyze concentration transients in different regions of the canyon and quantify peculiar behaviors deviating from the mean steady-state values.

The study is organized as follows. Section 2.1 presents the box model accounting for both transport and chemical dynamics. The results for the case of an inert gas emission with different time forcings at the source are presented in Section 3.1. The analysis will then extend to the emission of $NO_x$ 3.2. Finally, the conclusions of this work will be discussed in Section 4.

## 2. Methods

### 2.1. Model description

In European urban environments, street geometries commonly exhibit height to width aspect ratios ($H/W$) ranging from 0.5 to 2 (Soulhac and Salizzoni, 2010). Considering that the most elevated pollution levels occur in deep streets, our study specifically focuses on the upper limit of this range, which corresponds to a narrow canyon with an aspect ratio of $H/W = 2$. For this geometry, and for a

perpendicular incoming wind, the flow field (Fig. 1.a-b) is characterized by two overlapping vortices as well-documented by previous experimental (Fellini et al., 2020a) and numerical studies (Kovar-Panskus et al., 2002). The works of Salizzoni (2006); Salizzoni et al. (2009); Murena et al. (2011); Fellini et al. (2020a) have shown that a model with two degrees of freedom is suitable to describe pollutant exchanges within these types of canyons. This implies that the cavity wash-out can be accurately modelled by means of a sequence of pollutant transfers between three regions (Fig. 1.c-d): (i) the external flow, (ii) the recirculating cell at the top of the cavity (box 1) exchanging pollutants with the external flow, and (iii) the cell at the bottom of the cavity where pollutants are released (box 2).

Following this modelling approach, and assuming an absence of lateral street intersections (i.e., considering the canyon to be indefinitely long), the mass balance for the two boxes within the canyon reads:

$$\begin{cases} V_1 \dfrac{dC_1}{dt} = & S_{1e}u_{1e}(C_e - C_1) + S_{12}u_{12}(C_2 - C_1) + P_1 - D_1 \\ V_2 \dfrac{dC_2}{dt} = & S_{12}u_{12}(C_1 - C_2) + P_2 - D_2 + Q, \end{cases} \tag{1}$$

where $S_{1e}$ is the exchange surface between box 1 and the external flow and $S_{12}$ is the exchange surface between box 1 and box 2; $V_1$ and $V_2$, $C_1$ and $C_2$, $P_1$ and $P_2$, and $D_1$ and $D_2$, are the volume, mean concentration, production and destruction terms of box 1 and box 2, respectively. The emission $Q$ is located in the lower box (box 2). The bulk exchange velocities (see Appendix A for the definition) between box 1 and the external flow and between box 1 and box 2 are denoted as $u_{1e}$ and $u_{12}$, respectively. In this model, the street properties are assumed to be fairly uniform along the longitudinal axis of the canyon, and thus the geometry and the dynamics are assumed to be two-dimensional. Volumes and surfaces will then be considered per unit length along the canyon axis.

Setting the volume of each box as a function of the total volume of the cavity by means of a single geometrical parameter $\beta$ (i.e., $V_1 = \beta V$, $V_2 = (1-\beta)V$), and replacing the exchange surfaces (per unit length) $S_{1e}$ and $S_{12}$ equal to the width of the canyon, $W$, the characteristic time for pollutants to exit box 1 and box 2 can be defined as:

$$T_1 = \frac{\beta V}{W u_{1e}}, T_2 = \frac{(1-\beta)V}{W u_{12}}. \tag{2}$$

These equations show that the characteristic washout times depend on the exchange rates at the interfaces ($u_{1e}$ and $u_{12}$) and on the flow field topology inside the canyon, i.e. the size of the two recirculation cells that is described by the repartition parameter $\beta$. Recent studies (Salizzoni et al., 2009; Fellini et al., 2020a) have revealed that the vertical exchange rate at the canyon roof ($u_{1e}$) is governed by the intensity of the turbulent kinetic energy in the shear layer that develops at the interface between the external atmospheric flow and the flow in the cavity. The exchange between the two cells ($u_{12}$), instead, mainly depends on the turbulent kinetic energy that penetrates inside the canyon from the external flow. The exchange time $T_1$ can thus be considered as representative of the external atmospheric forcing and is in general shorter than $T_2$. For fixed external conditions, the ratio $T_2/T_1$ depends on the turbulent flow field inside the canyon: a high $T_2/T_1$ ratio occurs when the intensity of the turbulent kinetic energy entering the canyon is low compared to the turbulence intensity in the shear layer. This could be due to the presence of obstacle in the streets (such as tree crowns) or buoyancy effects a the lateral walls (Fellini et al., 2020a). Under these conditions, the washout time is much longer at pedestrian level where high levels of pollution will occur. Conversely, a low $T_2/T_1$ ratio reveals the presence of efficient turbulent transport within the canyon and

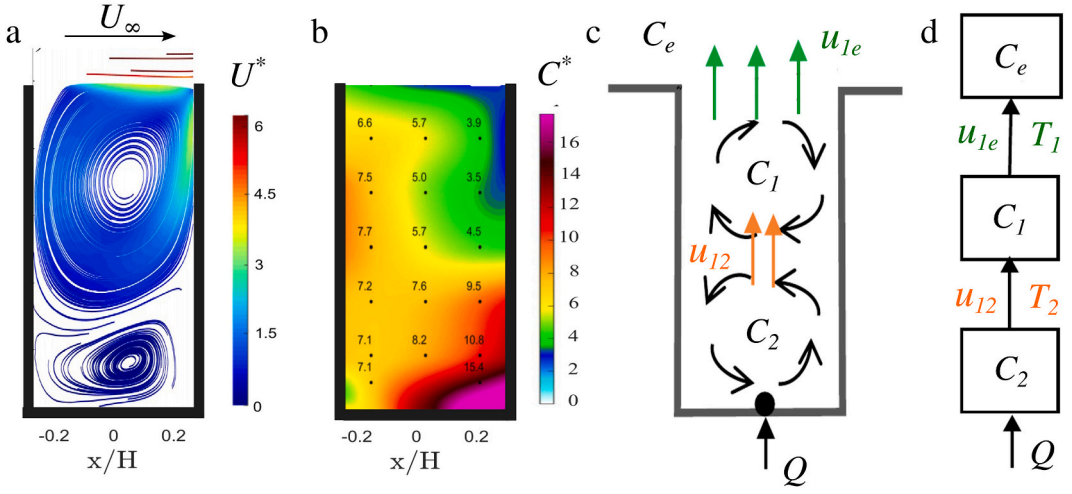


**Fig. 1.** a) Streamlines of the mean dimensionless velocity field $U^* = \left(U^2 + W^2\right)^{0.5}/u^*$ ($U$ and $W$ are the mean horizontal and vertical velocities, $u^*$ and $U_\infty$ are the friction and free stream velocities of the external boundary layer) and b) mean dimensionless concentration field ($C^* = Cu^*HL/Q$, where $L$ is the canyon longitudinal length) within a street canyon with height to width aspect ratio $H/W = 2$ from the experimental work of (Fellini et al., 2020a). c) Simplified representation of pollutant transfer dynamics inside the canyon with street emission $Q$. d) Schematic representation of the two-box model.

therefore more effective ventilation at street level.

By replacing Eqs. 2 in the concentration budgets (Eqs. 1), the two-box model becomes:

$$\begin{cases} \dfrac{dC_1}{dt} = & \dfrac{C_e - C_1}{T_1} + \dfrac{\alpha}{T_2}(C_2 - C_1) + p_1 - d_1 \\ \dfrac{dC_2}{dt} = & \dfrac{1}{T_2}(C_1 - C_2) + p_2 - d_2 + q, \end{cases} \tag{3}$$

where $\alpha = (1-\beta)/\beta$, while $q$, $p$ and $d$ are the source, chemical production and destruction per unit volume, respectively.

To introduce chemical transformations of nitrogen oxides in the box model, we use a minimalistic 3-reaction cycle for NO-$NO_2$-$O_3$ (see Appendix B). Despite the model's simplicity, its effectiveness in capturing the essential aspects of chemical dynamics has been confirmed in prior research. For instance, Bright et al. (2013) employed Large Eddy Simulation (LES) initially coupled with a basic 3-reaction scheme and later with a detailed chemical reaction mechanism (Reduced Chemical Scheme) involving 51 chemical species and 136 reactions. Their findings showed that increasing chemical complexity, such as simulating VOC chemistry, led to additional but modest formation of $NO_2$ and $O_3$ in the canyon. This numerical outcome aligns with the results presented in Soulhac et al. (1), where the outcomes of the 3-reaction chemical model were compared with measurements conducted in three urban canyons in the city of Lyon. Modelling the photolysis of $NO_2$ into NO and $O_3$ by means of the kinetic constant of reaction $k_1$, and the regeneration of $NO_2$ from NO and $O_3$ by means of the kinetic constant of reaction $k_3$, the production ($p$) and destruction ($d$) terms can be written according to the expressions reported in Eqs. B.12 in Appendix B. The mass balance for each chemical species ($NO_2$, NO, $O_3$) in the two boxes of the cavity results:

$$\begin{cases} \dfrac{d[NO_2]_1}{dt} = & -\dfrac{[NO_2]_1}{T_1} + \dfrac{\alpha}{T_2}\left([NO_2]_2 - [NO_2]_1\right) + k_3[NO]_1[O_3]_1 - k_1[NO_2]_1 \\ \dfrac{d[NO_2]_2}{dt} = & \dfrac{1}{T_2}\left([NO_2]_1 - [NO_2]_2\right) + k_3[NO]_2[O_3]_2 - k_1[NO_2]_2 + q_{NO_2} \\ \dfrac{d[NO]_1}{dt} = & -\dfrac{[NO]_1}{T_1} + \dfrac{\alpha}{T_2}\left([NO]_2 - [NO]_1\right) + k_1[NO_2]_1 - k_3[NO]_1[O_3]_1 \\ \dfrac{d[NO]_2}{dt} = & \dfrac{1}{T_2}\left([NO]_1 - [NO]_2\right) + k_1[NO_2]_2 - k_3[NO]_2[O_3]_2 + q_{NO} \\ \dfrac{d[O_3]_1}{dt} = & \dfrac{[O_3]_e - [O_3]_1}{T_1} + \dfrac{\alpha}{T_2}\left([O_3]_2 - [O_3]_1\right) + k_1[NO_2]_1 - k_3[NO]_1[O_3]_1 \\ \dfrac{d[O_3]_2}{dt} = & \dfrac{1}{T_2}\left([O_3]_1 - [O_3]_2\right) + k_1[NO_2]_2 - k_3[NO]_2[O_3]_2 + q_{O_3}, \end{cases} \tag{4}$$

where $[\cdot]$ represents the molar concentration (mol/$m^3$) of the compound, and their subscript 1, 2 and $e$ indicate the concentration in box 1, in box 2, and in the external flow, respectively. The emissions $q_{NO_2}$, $q_{NO}$ and $q_{O_3}$ are the emission rates per unit volume of $NO_2$, NO, and $O_3$, respectively. Since ozone is a secondary pollutant, its direct emission in the street can be neglected ($q_{O_3} = 0$) while the contribution from the external atmosphere (where indirect formation of $O_3$ occurs) is significant. For this reason, its concentration above roof level ($[O_3]_e$) is included in the model. Nitrogen monoxide and dioxides are instead directly emitted by the vehicular traffic and, in busy street canyons, this emission dominates with respect to the background contribution, that is here neglected. Their emission rates can be estimated as a function of the total $NO_x$ emissions ($q_{NO_x} = q_{NO_2} + q_{NO}$) by means of the repartition ratio $a = q_{NO_2}/q_{NO_x}$.

### 2.2. Simulated street canyon and emission scenarios

We focus on a realistic 10 m wide ($W$) street canyon, flanked by 20 m high buildings ($H$), with a main recirculating vortex occupying 70% ($\beta$) of the upper canyon volume (box 1), and a second smaller vortex in the bottom of the canyon (box 2). The vertical exchange velocities $u_{1e}$ and $u_{12}$ are fixed equal to 0.1 and 0.05 m/s, respectively, which are reasonable values for this geometry and are in accordance with previous experimental measurements (Fellini et al., 2020a). According to Eqs. 2, the ventilation times for the two boxes are $T_1 = 140$ s and $T_2 = 120$ s.

We examine a scenario characterized by clear skies ($Cld = 0$), a temperature of $\Theta = 20^{\circ}C$, and a solar elevation angle ($\chi$) of 45°. The background $O_3$ concentration is 170 $\mu g/m^3$. This setting is representative of a typical sunny day in Southern European cities during the spring season. According to Eq. B.11, the chemical transformation rates are computed as $k_1 = 8 \times 10^{-3}\,s^{-1}$ and $k_3 = 2.1 \times 10^{-4}\,m^3\mu g^{-1}s^{-1}$. Two characteristic time scales associated with the chemical transformations are then defined: $\tau_1 = 1/k_1$ and $\tau_3 = 1/(k_3[O_3]_e)$. In this scenario, $\tau_1$ is 125 s ($\tau_1/T_1 = 0.9$) and $\tau_3$ is 28 s ($\tau_3/T_1 = 0.2$). It is worth noting that these time scales are comparable to the characteristic ventilation times of the canyon ($T_1$ and $T_2$). Under these conditions, it becomes crucial to model both the transport and chemical transformation dynamics to obtain an accurate estimation of the pollution levels within the canyon.

The pollutant source is ground-level $NO_x$ vehicular emission, assumed to range from 0.5 to 300 $\mu g/m/s$. This range has been established based on findings from two prior studies related to traffic within street canyons in European city centers. The first study,

conducted by Soulhac et al. (2012), estimated $NO_x$ emissions in a district of Lyon, France, by employing traffic simulation and data derived from direct traffic measurements. Subsequently, the COPERT III model was applied. The second study, detailed in Li et al. (1) and Grylls et al. (2019), estimated $NO_x$ vehicular emissions in the urban district of South Kensington, London, through the coupling of VISSIM traffic microsimulation (Bloomberg and Dale, 2000) and the emission model developed by Panis et al. (2006). The emission per unit length estimated from these studies is then converted into an emission per unit volume (with the mean denoted as $q_0$ in the following). This conversion involves dividing by the volume of the bottom box ($V_2$) of the canyon, as specified by Eq. 3. The repartition of $NO_x$ at the emission is taken constant in this study and described by the repartition coefficient $a = q_{NO_2}/q_{NO_x}$ equal to 0.2 (Carslaw et al., 2016).

To replicate vehicular emissions, we progressively introduce emission models with increasing complexity in this study. Initially, we consider a constant emission over time. Subsequently, we shift to periodic emission signals, as vehicular emissions exhibit periodic patterns influenced by factors such as the typical travel time of a single car along the street (under low traffic conditions) or the regulation of a traffic light (under heavy traffic conditions).

For simulating this periodicity, we first model the emission as a sinusoidal function:

$$q(t) = q_0\left(1 + A sin\left(\frac{2\pi}{\tau}t\right)\right), \tag{5}$$

where $\tau$ is the period of the signal and $A$ is the coefficient that controls the amplitude of the periodic variations. The mean and the standard deviation of the sine function are $\mu = q_0$ and $\sigma = q_0 A/\sqrt{2}$, respectively. The parameters of the periodic emission are set as $\tau = 120$ s and $A = \sqrt{2}/3$. The period of the source $\tau$ is chosen as representative of the cycle length of a traffic light, while the amplification coefficient $A$ is fixed to match realistic emission variations around the mean and to facilitate the comparison with the stochastic emission scenario. Adopting this value for $A$, the standard deviation and the coefficient of variation (CV $= \sigma/\mu$) of the source are $\sigma = q_0/3$ and CV $= 1/3$, respectively.

Finally, we take into account the non-deterministic nature of vehicular emissions due to many unpredictable factors like driving behavior, variations in the intensity of the vehicular traffic, and the turbulent nature of the wind in the street canyon. To address these variabilities, the source signal is forced with a coloured Gaussian noise $X(t)$, (i.e)

$$q(t) = q_0 + X(t), \tag{6}$$

**Table 1**
Street canyon parameters and variability ranges simulated in this study.

| Geometrical parameters | | | | |
|---|---|---|---|---|
| Width & Height | W [m] | 10 | H [m] | 20 |
| Flow dynamics parameters | | | | |
| Topology of cells | $\beta$ [·] | 0.7 | $\alpha$ [·] | 0.43 |
| Vertical bulk velocities | $u_{1e}$ [m/s] | 0.1 | $u_{12}$ [m/s] | 0.05 |
| Ventilation times | $T_1$ [s] | 140 | $T_2$ [s] | 120 |
| Emission parameters | | | | |
| Emission mean for inert gas | $Q_0$ [μg/m/s] | 45 | $q_0$ [$\mu g/m^3/s$] | 0.75 |
| Emission mean for $NO_x$ | $Q_0$ [$\mu g/m/s$] | 60 | $q_0$ [$\mu g/m^3/s$] | 1 |
| Repartition coefficient for $NO_x$ | $a$ [·] | 0.2 | | |
| Emission period | $\tau$ [s] | 120 | | |
| Emission time variability | $\sigma_q$ [$\mu g/m^3/s$] | $q_0/3$ | $CV_q$ [·] | 1/3 |
| Chemical parameters | | | | |
| Reaction rates | $k_1$ [$s^{-1}$] | $8 \times 10^{-3}$ | $k_3$ [$m^3/\mu g/s$] | $2.1 \times 10^{-4}$ |
| Reaction time scales | $\tau_1$ [s] | 125 s | $\tau_3$ [s] | 28 s |
| Background $O_3$ concentration | $C_{O3}$ [$\mu g/m^3$] | 170 | | |
| Range of varying parameters | | | | |
| Emission mean (unit length) | $Q_0$ [$\mu g/m/s$] | 0.5–300 | | |
| Emission mean (unit volume) | $q_0$ [$\mu g/m^3/s$] | 0.01–5 | | |
| Ventilation time (bottom box) | $T_2$ [s] | 35–130 | | |
| Emission period | $\tau$ [s] | 40–220 | | |
| Reaction time scale 1 | $\tau_1$ [s] | 14 - $1.4 \times 10^4$ | | |
| Reaction time scale 3 | $\tau_3$ [s] | 14–280 | | |
| Range of time ratios | | | | |
| Ventilation time ratio | $T_2/T_1$ [·] | 0.25–0.93 | | |
| Emission period | $\tau/T_1$ [·] | 0.3–1.6 | | |
| Reaction time scale 1 | $\tau_1/T_1$ [·] | 0.1–100 | | |
| Reaction time scale 3 | $\tau_3/T_1$ [·] | 0.1–10 | | |

which accounts for random fluctuations at the emission but maintains a characteristic temporal scale. The noise is obtained from the Ornstein-Uhlenbeck process and its main parameters are the relaxation time, $\tau$, and the diffusion constant of the process, $\varepsilon$. The diffusion constant amplifies the noise, while the relaxation time is representative of the autocorrelation of the signal, that mimics the periodicity of vehicle transits. For $\tau \to 0$ the signal tends to a Gaussian white noise, i.e. a completely uncorrelated noise. The stochastically perturbed emission is obtained by summing the noise $X(t)$ to the mean emission $q_0$. As a result, the emission is characterized by a Gaussian $NO_x$ function, with mean $q_0$ and variance $\varepsilon\tau/2$ (see Appendix C for details). To limit negative entries for the source signal, we choose the diffusion constant $\varepsilon$ in such a way that nearly all values lie within three standard deviations of the mean:

$$3 \cdot \mathrm{std}\{X(t)\} = q_0 \to \varepsilon = \frac{2}{9}\frac{q_0^2}{\tau}. \tag{7}$$

As a further control, rare negative occurrences for $q$ are forced to be equal to zero. Thus, the source term has mean $q_0$, standard deviation $q_0/3$ and CV $= 1/3$, as the sinusoidal emission described above.

The parameter values considered in this study are summarized in Table 1. To explore the impact of different characteristic time scales for both transport and chemistry on concentration dynamics within the canyon, we systematically vary the characteristic exchange time between the bottom and upper boxes ($T_2$), the characteristic emission period ($\tau$), and the timescales associated with chemical reactions ($\tau_1$ and $\tau_3$). Additionally, we examine the variation in emission intensity ($q_0$). The specified parameter ranges are presented at the end of Table 1. For emissions, we referred to the same studies mentioned above (e.g., Soulhac et al., 2012). Regarding the ventilation time $T_2$, we considered a reasonable sensitivity based on previous experimental works (Fellini et al., 2020a). For reaction times, we took into account the reasonable sensitivity of meteorological parameters determining $k_1$ and $k_3$.

## 3. Results

### 3.1. Inert gas

#### 3.1.1. Deterministic emissions

We begin by examining a straightforward scenario in which there are no chemical transformations ($p = d = 0$), the emission remains constant over time ($q = q_0$), and the air pollutant concentration above roof level is significantly lower than the pollution inside the canyon (i.e., $C_e - C_1 \simeq -C_1$). This condition is valid for pollutants primarily emitted directly into the streets (e.g., $NO_2$ and NO from vehicular traffic), where the atmosphere above the rooftops acts as a dilution factor. However, this assumption may not be applicable to other pollutant types, such as ozone or particulate matter, where external deposition into the canyon is not negligible.

Under these assumptions, the numerical solution of the system in Eq. 3 provides the temporal pattern of the concentration in the two boxes (Fig. 2.a). The coloured lines depict the concentration transient from an initial state ($C_1(0),\ C_2(0)$) as a function of the source intensity and show that the concentration of pollutants can reach a maximum value during the transient phase greater (even by a factor of two) than the initial or final state. The concentration values at final solution lie on straight lines with slope $1 + T_2/(\alpha T_1) = 1 + u_{1e}/u_{12}$. These are represented for different $T_1/T_2$ ratios as dashed and continuous lines in Fig. 2.a. This result correspond to the analytical solution of Eq. 3 at steady state:

$$\begin{cases} C_{0,1} = & \alpha T_1 q_0 \\ C_{0,2} = & (\alpha T_1 + T_2) q_0. \end{cases} \tag{8}$$

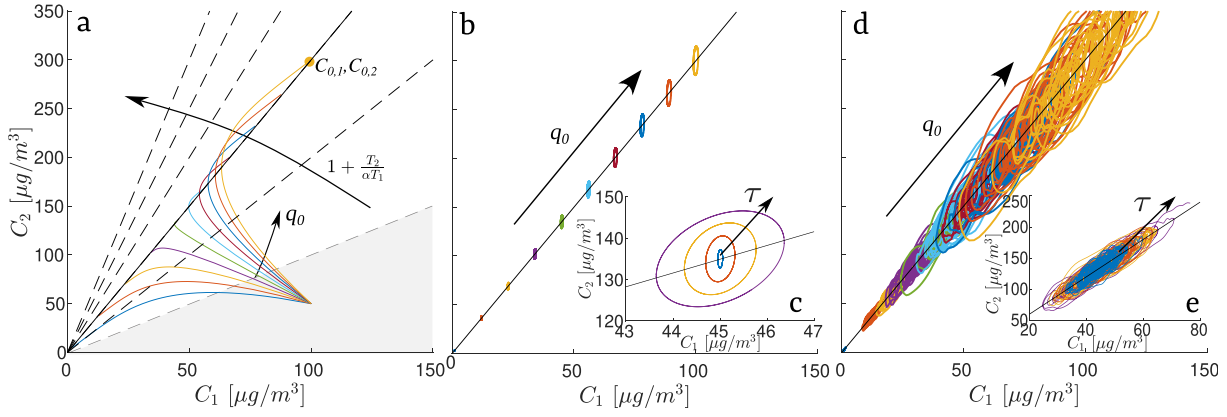


**Fig. 2.** (a) Concentration transients in the space $\{C_1, C_2\}$ for a constant emission with varying intensity $q_0$. The steady state solutions lie on straight lines with slope $1 + T_2/(\alpha T_1)$ (continuous line for the case study, dashed lines for the possible solutions with varying $T_2/(\alpha T_1)$). (b-c) Steady state limit cycles in the space $\{C_1, C_2\}$ for (b) periodic emissions with constant $\tau$ and varying intensity $q_0$, and for (c) periodic emissions with constant $q_0$ and varying period $\tau$. (d-e) Noisy solution for (d) stochastic emissions with constant $\tau$ and varying intensity $q_0$, and for (e) stochastic emissions with constant $q_0$ and varying period $\tau$.

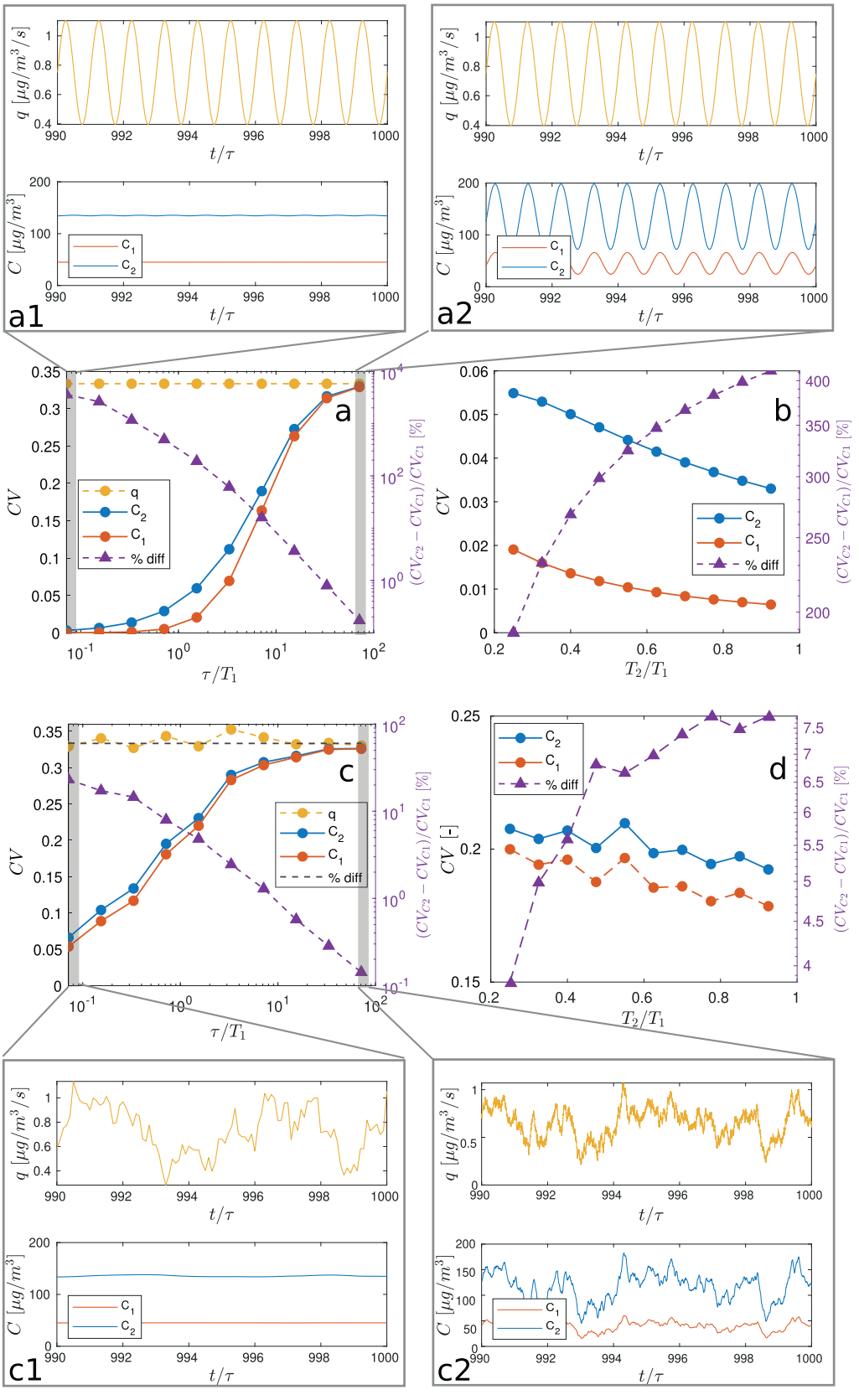


*(caption on next page)*

**Fig. 3.** Inert gas. a) Coefficient of variation (CV) of the source ($q$) and concentration signals ($C_1$ and $C_2$) as a function of $\tau/T_1$ for a periodic emission. Panels (a1) and (a2) show the emission and concentration signals over time for $\tau/T_1 = 0.07$ and $10^2$. b) CV as a function of $T_2/T_1$ for a periodic emission. c) CV as a function of $\tau/T_1$ for a stochastic emission. Panels (c1) and (c2) show the emission and concentration signals over time for $\tau/T_1 = 0.07$ and $10^2$. d) CV as a function of $T_2/T_1$ for a stochastic emission. In a and b, the grey dashed line is the theoretical CV from the derived distributions for $C_1$ and $C_2$.

When the level of turbulent kinetic energy within the street canyon is so high that the internal ventilation rate is comparable with the exchange rate in the shear layer (i.e. $u_{12} \approx u_{1e}$), the ratio $T_2/(\alpha T_1)$ approaches 1, resulting in the concentration in the bottom box being twice that in the upper box. The scenario with equal concentrations in both boxes (a solution that aligns with the bisector of the graph, grey dashed line in Fig. 2) is realized when the ratio $T_2/(\alpha T_1)$ approaches zero. In this context, the exchange between the two boxes occurs so rapidly that the ratio $T_2/T_1$ tends to 0. Conversely, as the internal transfer of pollutants is inhibited (low $u_{12}$), the concentration at street level ($C_2$) increases with respect to the concentration in the upper part of the canyon, i.e. the steady solution $(C_{0,1}, C_{0,2})$ lies on a straight line with increasing slope.

To simulate emissions from vehicular traffic, a non-constant emission pattern with a periodic trend (refer to section 2.2) is incorporated into the system described by Eq. 3 and subsequently numerically solved. The obtained results are illustrated in Fig. 2.b. The solution is asymptotically stable and forms a limit cycle in the space $\{C_1, C_2\}$. As $q_0$ increases, both the mean concentration and the amplitude of the concentration oscillations in the two boxes increase, and the centroid of the ellipse moves along the straight line with slope $1 + T_2/(\alpha T_1)$. When $q_0$ is fixed and $\tau$ is increased, the amplitude of the concentration fluctuations increases as well, as shown by the growing size of the limit cycles in Fig. 2.c. This is confirmed by Fig. 3.a that reports the trend in the coefficient of variation (CV) for the source and for the concentration in the two boxes as a function of the source period, $\tau$. The source signal (yellow line) is characterized by the highest CV (equal to 1/3, see section 2.2), while concentration fluctuations (blue and orange lines) are damped by the dynamics in the two boxes. These damping effects are maximized when the source emission is high frequency, while they decrease as $\tau/T_1$ increases. When the period of the source is very short compared to the characteristic time of the system (low $\tau/T_1$), the system does not "have the time" to react to the source fluctuations and settles on the mean concentration value and the coefficient of variation for the concentration tends to zero. This behavior is evident from the temporal patterns of both emission and concentration, as depicted in panel a1 of Fig. 3. On the other hand, when the source oscillations are very slow (high $\tau/T_1$), the system follows the emission variations and the concentrations in the two boxes vary with the emission as a succession of stationary states, as shown in panel a2. In this case, the coefficient of variation for the concentration tends to that of the source. The graph also highlights that the CV for the concentration increases with $\tau/T_1$ following a sublinear trend (approximately logarithmic for intermediate values of the $\tau/T_1$ range).

The bottom box (i.e. box 2 where the source is located) acts as an additional low-pass filter for the upper box (box 1) that experiences weaker concentration variations. It is worth noting that for the concentration coefficient of variation (CV) to be approximately equal in both boxes and equivalent to that of the emission, the period of the source should be at least two orders of magnitude greater than the exchange time $T_1$ (i.e., $\tau/T_1 \gtrsim 100$).

The analysis also reveals that the concentration signals have the same period of the source but, as $\tau$ increases, the time shift ($\Delta t$) between $C_2$ and $q$ and between $C_1$ and $C_2$ increases as well, while the phase shift ($\Delta\Phi = \Delta t 2\pi/\tau$) decreases (Fig. 4). For $\tau \to \infty$ the three signals tend to be synchronized since both $T_1$ and $T_2$, that govern the dynamics between boxes, become negligible with respect to the forcing period. Synchronized concentration signals implies that the maximum (and the minimum) pollution intensity for the two

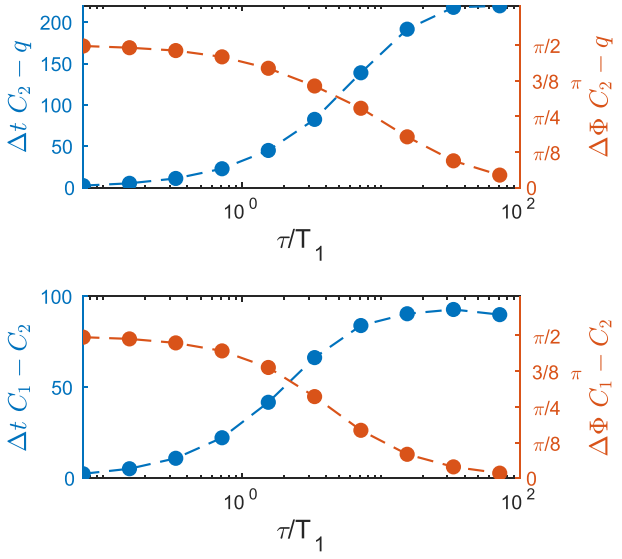


**Fig. 4.** Time (left axis) and phase (right axis) shift between $q$ and $C_2$ (first panel) and between $C_1$ and $C_2$, as a function of the emission period $\tau$, for an inert gas.

regions of the canyon is reached at the same time, i.e. at the time of maximum release from the source. The clockwise rotation of the ellipse axis in Fig. 2.c is another marker of the change in the phase shift between $C_1$ and $C_2$ with $\tau$. As $\tau$ increases, the ellipse stretches over the straight line with slope $1 + T_2/(\alpha T_1)$. This indicates that the period of the source is so long that the concentration in the two boxes reaches intermediate states that correspond to the concentration that would occur with steady emissions with intensity varying between $q_0(1 - A)$ and $q_0(1 + A)$, that is the range of variation of the sinusoidal emission.

The effect of the wash-out times is significant for the mean pollution levels but not for the concentration oscillations (Fig. 3.b). In this regards, Fig. 3.b reveals that the inhibition of the vertical mixing between the two boxes (i.e. the increase of $T_2/T_1$) tends to reduce the coefficient of variation in the entire canyon and to increase the damping effect of box 2 on box 1 (see the right axis in Fig. 3.b).

These results show that, for a deterministic emission, the mean pollution level within the street canyon depends on the mean release at the source and the characteristic wash-out times of the canyon. On the other hand, concentration peaks increase both with amplitude and the period of the emission. For a given source emission, air pollutant concentration significantly varies with distance from the street. In the lower part of the canyon, i.e. at the lower building floors, air pollutant concentrations are higher on mean and show the greatest peaks. On the upper floors both mean and peak concentrations are attenuated.

### 3.1.2. *Stochastic emissions*

To simulate realistic emissions from vehicular traffic, influenced by variations in driving behavior and dispersion in a turbulent wind environment, the stochastic emission pattern with autocorrelation $\tau$ (refer to section 2.2) is incorporated into the system described by Eq. 3 and subsequently numerically solved. The solution (Fig. 2.d) provides noisy concentration signals that (after an initial transient) are statistically stable in the space $\{C_1, C_2\}$. As $q_0$ increases, both the mean concentration and the amplitude of the concentration oscillations in the two boxes increase. The mean concentrations of $C_1$ and $C_2$ define a point in the space that moves along the straight line with slope $1 + T_2/(\alpha T_1)$. When $q_0$ is fixed and $\tau$ is increased the amplitude of the concentration fluctuations increases as well, as shown in Fig. 2.e. This effect is however less significant with respect to the case of the sinusoidal forcing (panel c). These results are confirmed by Fig. 3.c. The coefficient of variation for the concentration increases with $\tau/T_1$ with a non-linear trend (approximately logarithmic for $\tau/T_1 < 10$), and its value is significantly higher for the stochastic source than for the sinusoidal source when $\tau/T_1$ is lower than 30, so that the gradient of the curve is less marked.

As already found for the sinusoidal emission, the effect on the concentration fluctuations of the ratio $T_2/T_1$ at fixed $\tau$ is not marked (Fig. 3.d). Finally, we observe that the damping effect of box 2 on box 1 (right axis of panel c and d) is still noticeable and follows the same trends seen for the sinusoidal source (right axis of panels a and b). However, this dampening effect is considerably weaker, indicating that the stochastic nature of the emission tends to equalize the magnitude of fluctuations in the two boxes. As a result, the CV curves for the concentration in the two boxes are much closer when the stochastic source is considered.

To gather further insights into the dynamics of concentration within the canyon, we report in Fig. 5 the probability density function (*pdf*) of the source emissions, and of the concentrations $C_1$ and $C_2$, for different ratios $\tau/T_1$. While the Gaussian distribution is invariant for the source, the occurrence of extreme values for the concentration increases with $\tau/T_1$, while the mean value of the distribution remains the same, in line with the results found in Fig. 2.e and 3.c. For $\tau/T_1 \to \infty$, the ventilation process is much faster than the emission timescale, $\varepsilon$ approaches zero (see Eq. 7), and the emission noise varies so slowly that the concentration response of the system becomes independent of the period itself and the amplitude of the concentration variations follows the amplitude of the emission variations. As a consequence, the *pdf* of the concentration collapses onto that of the emission. Notice that in this case the *pdf* of the concentrations can be analytically found (see Appendix D) and are reported as dotted grey line in Fig. 5.b-c. On the other hand, for $\tau \to 0$, the system behaves as a filter for the noise at the source, and the coefficient of variation for the concentration tends to 0, i.e. the concentration tends to be steady over time (see also panel c1 in Fig. 3).

These results highlight that the stochastic nature of the source has no influence on the stability of the system that still provides a single (statistically) stable solution for the concentration in the two boxes. The concentration solution follows a noisy path around the mean value that is the same already found for the constant and sinusoidal source. The amplitude of the fluctuations around the mean

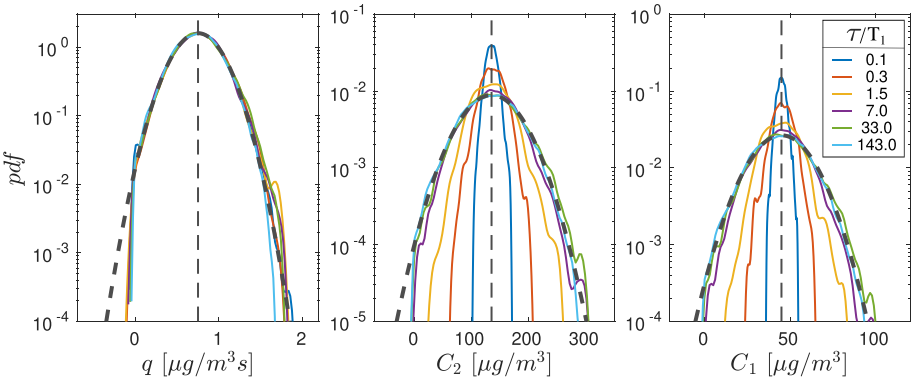


**Fig. 5.** Probability density function of the source and concentration signals for different values of the ratio $\tau/T_1$ (see the legend). The dotted curves are the Gaussian distributions found for $\tau/T_1 \to \infty$ (see Eqs. D.20-D.23). The dotted vertical lines are the means found from these distributions.

(described by the coefficient of variation) is greater the longer the memory of the signal. Moreover, the stochastic fluctuations noticeably amplify the concentration variations with respect to a deterministic emission with same periodicity ($\tau$), mean intensity ($q_0$) and standard deviation, while they tend to homogenize the coefficient of variation in the two boxes.

### 3.2. Reactive gas

#### 3.2.1. Deterministic emissions

For vehicular emissions constant in time (i.e., $q_{NO_x} = q_{NO} + q_{NO_2} = q_0$), the numerical solution of the system in Eq. 4 provides the steady and transient concentration of $NO_2$, NO, and $O_3$ in the two boxes, as reported in Fig. 6.a and b. The steady concentration (panel a) does not vary linearly with the emission intensity and $O_3$ is progressively depleted as $NO_x$ emissions increase. This is in line with previous works (e.g., Li et al., 2023) showing that the steady concentrations of the three chemical compounds follow a non-linear trend with the source emission when the background $O_3$ concentration is different from zero. Moreover, as expected, concentrations at street level (dashed lines) are about twice those at the top of the canyon (continuous lines) for NO and $NO_2$, while $O_3$ follows an inverse trend. The concentration of $O_3$ above roofs acts as a source that feeds the upper box, while the amount of $O_3$ transferred to street level is limited by the exchange between the two boxes (governed by the characteristic time $T_2$) and by the depletion of $O_3$ by reaction with the $NO_x$ emissions from vehicular traffic. Fig. 6.b reports the concentration transients for the three pollutants, starting from a fixed initial condition but varying the emission rate ($q_0$). Due to nonlinear chemical reactions, unlike the results shown for the passive scalar (see Fig. 2.a), the ratio between the steady concentrations in the two boxes is not constant, i.e. the steady concentration in the two boxes lies on curved lines in the space $\{C_1, C_2\}$ (see the dashed grey lines).

When the emission at the source is periodic (Fig. 6.c), the solution for each chemical species follows a limit cycle in the space $\{C_1,C_2\}$, in line with the results found for the inert gas (see Fig. 2.b-c). When the mean ($q_0$) and - as a consequence - the standard deviation ($\sigma = q_0/3$) of the emission of $NO_x$ increase, the mean and standard deviation of the concentration fluctuations increase for $NO_2$ and NO in the two regions of the canyon (blue and red circles in panel c of Fig. 6). On the other hand, the size of the ellipses representing the variations in $O_3$ concentration reaches a maximum for intermediate emission intensities of $NO_x$ since $O_3$ oscillations

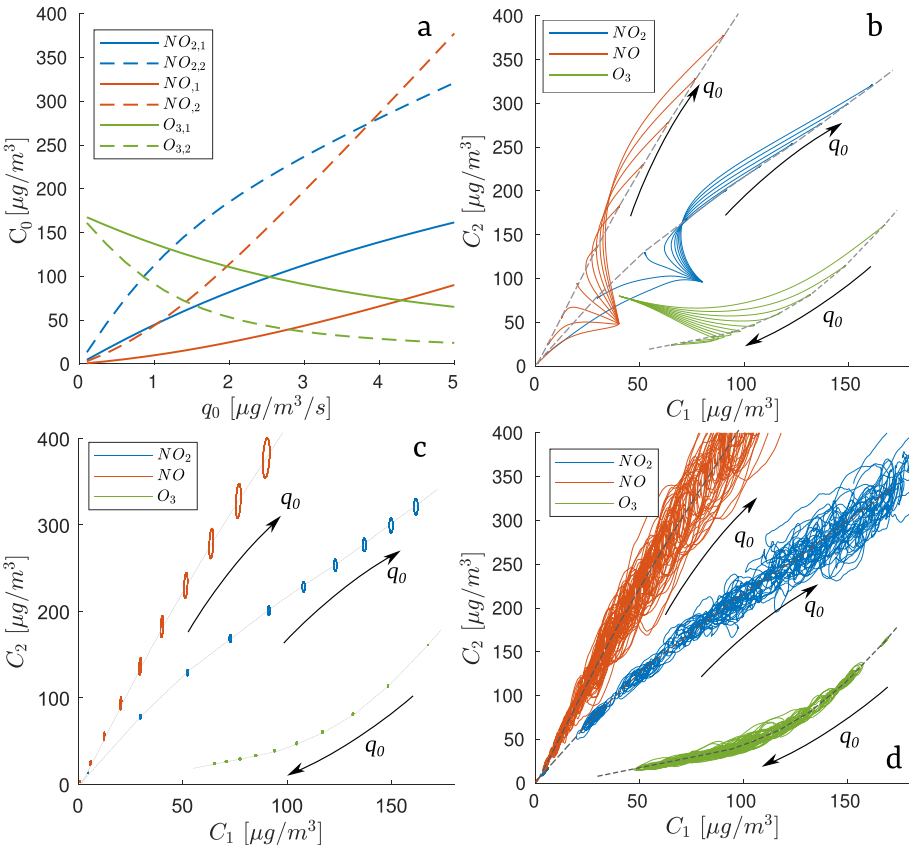


**Fig. 6.** a) Steady-state concentration of $NO_2 - NO - O_3$ as a function of the vehicular emissions $q_0$ in the upper part of the canyon (continuous lines) and at the bottom (dashed lines). b) Concentration transients in the space $\{C_1,C_2\}$ for varying $q_0$ ($q_0 = q_{NO} + q_{NO_2}$). The grey dashed lines correspond to the steady solution in the two boxes for varying $q_0$. c) Steady-state limit cycles in the space $\{C_1,C_2\}$ for periodic emissions with constant $\tau$ and varying $q_0$. d) Steady-state limit cycles in the space $\{C_1,C_2\}$ for stochastic emissions with constant $\tau$ and varying $q_0$.

are, on one hand, driven by the growing amplitude of $NO_x$ emissions (with $q_0$), but, on the other hand, they are constrained by the reduction of the mean $O_3$ concentration, due to chemical transformations.

Focusing on the effect of the source periodicity, we observe that, as $\tau/T_1$ increases, the mean concentration of the three chemical compounds does not change (Fig. 7.a), while their coefficient of variation (Fig. 8.a) increase significantly. This is in line with the results found for the inert pollutant in Fig. 3. It is interesting to observe in Fig. 8.a that concentration fluctuations of NO exceed those of the source when the period of the emission is very long compared to the characteristic time of street ventilation (i.e. $\tau \gg T_1$). This suggests that the chemical transformations reduce the mean concentration of NO which would settle in the canyon if it were an inert gas. This reduction of the mean implies an increase in the CV with respect to that observed in Fig. 3.a for an inert pollutant, which instead remains always below the CV of the source. Moreover, while the bottom box (where the source is located) acts as a low-pass filter for NO and $O_3$ concentrations, this is not always the case for $NO_2$.

As previously observed in the case of inert pollutants, when the vertical exchange between the lower and upper boxes slows down (increasing $T_2/T_1$), the concentration of the pollutants emitted by the source (NO and $NO_2$) increases in the bottom box (dashed lines in Fig. 7.b). This is responsible for the slight decrease in CV observed in Fig. 8.b. Mirroring $NO_x$, the mean $O_3$ concentration in the bottom box decreases with $T_2/T_1$ and the CV becomes three times larger. In the upper box, the mean concentration of the three chemical species remains unchanged with $T_2/T_1$ (continuous lines in Fig. 7.b), while the CV slightly decreases with it (Fig. 8.b). This suggests that the longer residence time of the pollutants in the bottom box, dampens the fluctuations transmitted to the upper box.

The time scales of the chemical reactions affect especially the mean concentration in the two boxes. The photolysis of $NO_2$ into NO and $O^{\bullet}$ (Eq. B.10) slows down $\tau_1$ increases. As a consequence, the mean concentration of $NO_2$ increases with $\tau_1/T_1$ at the expense of a reduction in NO and $O_3$ (see Fig. 7.c). As $\tau_3$ increases, the regeneration of $NO_2$ from NO and $O_3$ reaction is inhibited, the mean concentration of $NO_2$ decreases while $O_3$ and NO increase (see Fig. 7.d). These variations of the mean are reflected in the trends for the CV of the three chemical compounds (Figs.8.c-d).

The analysis of the probability density function (*pdf*) of air pollutant concentration for the three chemical compounds reveals additional interesting behaviors associated with the periodicity of the emission source, as depicted in Fig. S2 and Fig. S3 in the supplementary material (SM, hereafter). As expected for a system forced by a sinusoidal signal, the *pdf* of the concentration is bimodal with two peaks occurring at the maximum and minimum concentration values. Despite the emission being driven by a symmetric sinusoidal signal, the concentration distributions display asymmetry with respect to the mean as $\tau/T_1$ increases. This departure from symmetry is certainly due to the non-linearity introduced by the chemical transformations and is confirmed by the non-zero skewness

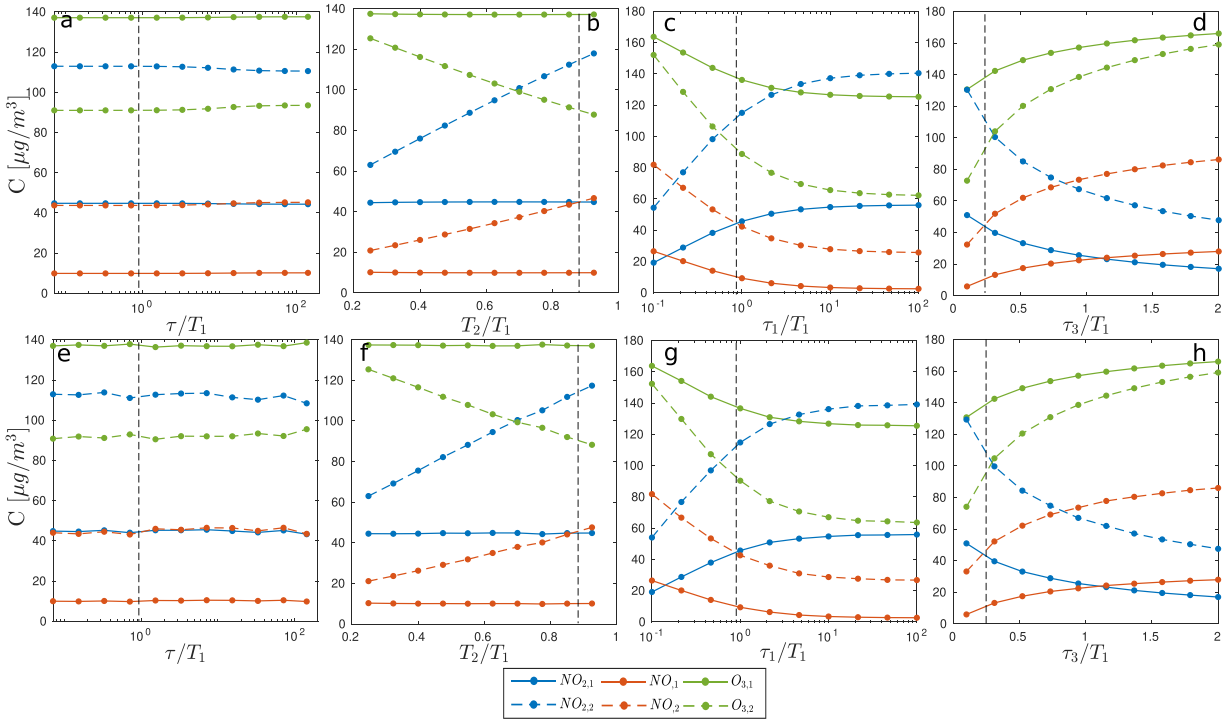


**Fig. 7.** Mean concentration for the three chemical species in the bottom box (dashed lines) and upper box (continuous lines) of the canyon. The first row reports the mean concentration as a function of $\tau/T_1$ (a), $T_2/T_1$ (b), $\tau_1/T_1$ (c), and $\tau_3/T_1$ (d) for a deterministic periodic emission. The second row reports the mean concentration as a function of $\tau/T_1$ (e), $T_2/T_1$ (f), $\tau_1/T_1$ (g), and $\tau_3/T_1$ (h) for a (coloured) stochastic emission. The graphs of the standard deviation are reported in the Supplementary Material. The characteristic times of the system (see Table 1) are reported as vertical dashed black lines.

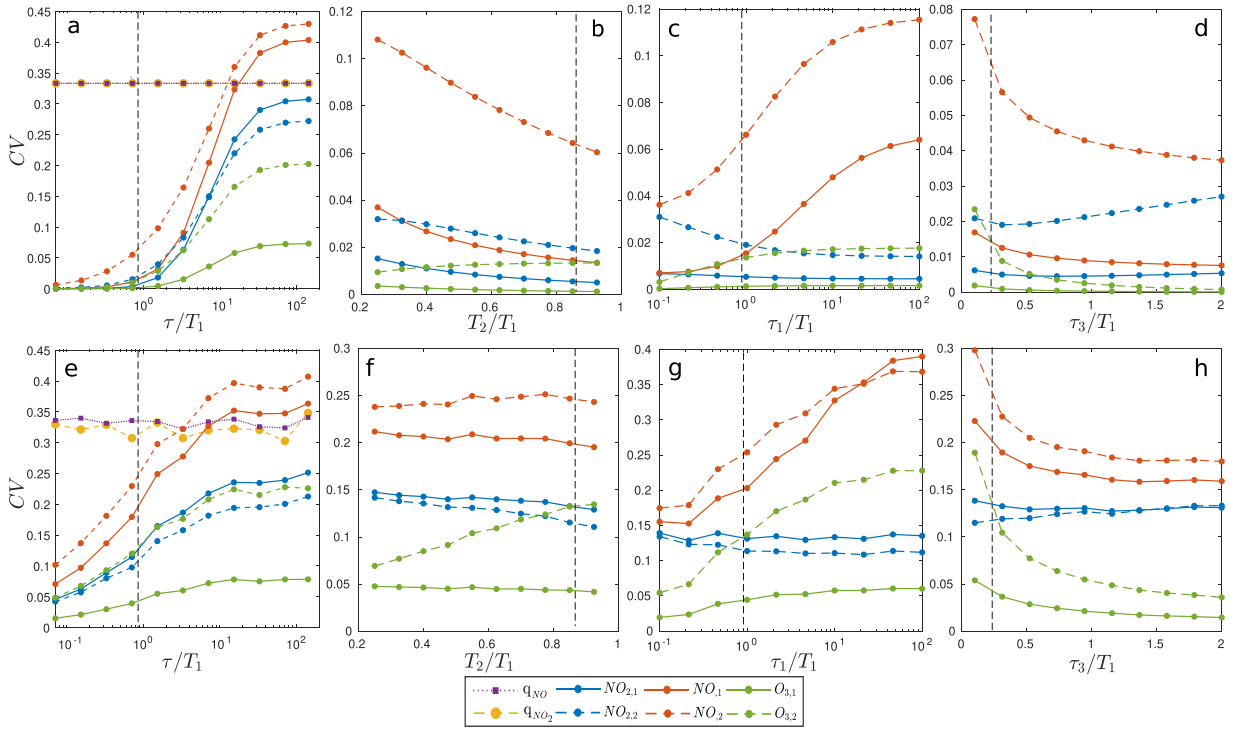


**Fig. 8.** Coefficient of variation (CV) of the source ($q_{NO}$ and $q_{NO2}$) and concentration signals in the bottom box (dashed lines) and upper box (continuous lines) of the canyon. The first row reports the CV as a function of $\tau/T_1$ (a), $T_2/T_1$ (b), $\tau_1/T_1$ (c), and $\tau_3/T_1$ (d) for a deterministic periodic emission. The second row reports the CV as a function of $\tau/T_1$ (e), $T_2/T_1$ (f), $\tau_1/T_1$ (g), and $\tau_3/T_1$ (h) for a (coloured) stochastic emission. The characteristic times of the system (see Table 1) are reported as vertical dashed black lines.

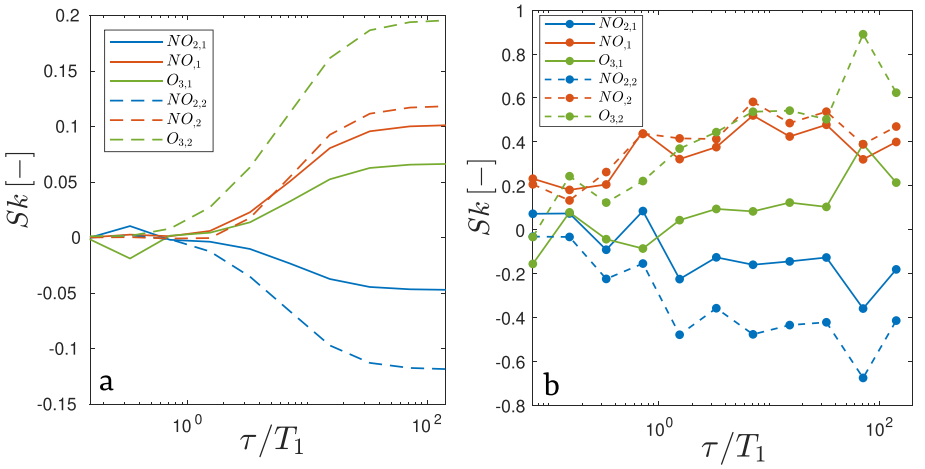


**Fig. 9.** Skewness of $NO_2$ (blue line), NO (orange line), and $O_3$ (green line) in the bottom box (dashed lines) and upper box (continuous lines) of the canyon, for different emission timescales ($\tau/T_1$). a) Sinusoidal forcing. b) Stochastic forcing. (For interpretation of the references to colour in this figure legend, the reader is referred to the web version of this article.)

of the concentration signal (Fig. 9). More specifically, the distributions for $NO_2$ tend to exhibit negative skewness, indicating a higher frequency of lower concentrations. On the other hand, the distributions for NO and $O_3$ tend to have a right tail, i.e. high concentrations of pollutants become more frequent with respect to the mean. It is expected that this behavior becomes more pronounced as $\tau/T_1$ increases since, as mentioned earlier, the system is more sensitive to oscillations when the emission has a long characteristic period. Conversely, when $\tau/T_1$ is very small, the system filters out the oscillations at the source, resulting in little deviation of the pollutant concentration from its mean value.

### 3.2.2. Stochastic emissions

The emission of NO and $NO_2$ are randomly and independently perturbed with a coloured Gaussian noise (see section 3.1.2).

The simulation results in Fig. 6.d show that the concentration in the two regions of the canyon forms noisy limit cycles in the space $\{C_1, C_2\}$. The temporal scale of the source ($\tau$) has no effect on the mean concentration in the canyon (Fig. 7.e) but it considerably affects the amplitude of the concentration fluctuations around the mean (Fig. 8.e). The results are qualitatively similar to those found for the periodic source: (i) the concentration fluctuations increase with $\tau/T_1$, and (ii) the coefficient of variation of NO exceeds that of the source, (iii) the bottom box (where the source is located) acts as a low-pass filter for NO and $O_3$ concentration fluctuations, but not for $NO_2$. However, as already observed for the inert case (Fig. 3), the increase in the standard deviation (Fig. S1.e in the SM) and in the coefficient of variation (Fig. 8.e) with $\tau/T_1$ is much more rapid for the stochastic forcing than for the deterministic sinusoidal one (Fig. 8.a).

When the slowing down of the vertical exchange between the lower and upper boxes occurs (i.e., increase of $T_2/T_1$), the pollutants emitted by the source (NO and $NO_2$) accumulate in the bottom box (dashed lines in Fig. 7.f). However, differently from the deterministic case, also the standard deviation (dashed lines in Fig. S1.f in the SM) increases significantly with $T_2$ so that the CV is almost unaltered (Fig. 8.f). Mirroring $NO_x$, the mean $O_3$ concentration in the bottom box (dashed line in Fig. 7.f) decreases with $T_2/T_1$. The standard deviation (see Fig. S1.f in the SM) increases but less rapidly, so that the coefficient of variation (panel f in Fig. 8) increases up to three times when $T_2 \sim T_1$. In the upper box (continuous lines in Fig. 7.f) the mean concentration of the three chemical species remains unchanged with $T_2/T_1$, the standard deviation very slightly decreases and the CV with it (continuous lines in Fig. 8.f).

Beyond the trends observed with $T_2/T_1$, panel f, when compared to the sinusoidal source case (panel b), highlights that the coefficient of variation exhibits significantly higher values in the stochastic scenario (approximately three times higher). This finding aligns with the patterns observed in panel e when contrasted with panel a, as well as for the inert gas case, as indicated by the CV values in panels a and b compared to c and d in Fig. 3. This phenomenon can be attributed to the distinct shapes of the two probability distributions for source emission. Given the same CV, the stochastic case demonstrates longer tails, as illustrated in Fig. S5 in the SM. These extended tails indicate the presence of extremely low or high emission values, triggering a nonlinear system response that results in concentration extremes within the canyon. This, in turn, amplifies the standard deviation and, consequently, the CV of concentrations. This shows that the system's nonlinearity, coupled with random emission fluctuations, does not significantly impact the mean concentration but exerts notable effects on concentration extremes and, consequently, on citizens' exposure. We also remark that the stochastic fluctuations at the source tend to reduce the differences in standard deviation (and therefore in CV) between the two boxes, as already observed for non-reactive pollutants.

The effect of the time scales of the chemical reactions on the mean concentration is almost identical to that observed for the deterministic periodic source (see Fig. 7.g-h) while the standard deviation follows similar but not identical trends (Fig. S1.g-h in the SM). The non-trivial interplay of variations in standard deviation along with those in the mean is reflected in the trend of the coefficient of variation reported in panels g and h of Fig. 8. In this case as well, the CV values highlight the greater variability of concentrations in the stochastic source scenario (panels g-h) compared to the sinusoidal one (c-d).

The analysis of the probability density functions of the time series (Fig. S4 in the SM) reveals interesting patterns. First, it's worth noting that the *pdf*s are unimodal, unlike the bimodal distributions observed for the deterministic sinusoidal source. Secondly, as mentioned above, the tails of the stochastic emission distribution are much longer than those of the deterministic source (see Fig. S5 in the SM). Thirdly, the probability distributions in Fig. S4 extend over increasing ranges of values as $\tau$ increases. This confirms the results found in Fig. 8, namely that as emissions occur with longer time scales compared to the characteristic ventilation time, the concentration fluctuations in the street canyon become larger. Finally, similar to the deterministic case, Fig. S4 reveals a growing asymmetry in concentration values with respect to the mean as $\tau$ increases. This behavior is well summarized by the skewness of the distributions in Fig. 9.b. The trend, albeit more noisy, is consistent with the findings for the sinusoidal emission case.

## 4. Conclusions

This study has enhanced our understanding of the transport and transformation dynamics of reactive and inert pollutants in street canyons through a simplified modelling approach and innovative analysis using phase diagrams.

For a constant emission of an inert pollutant, we were able to evaluate the transient behavior leading to the steady-state concentration. The results showed that the ratio between the two characteristic exchange times ($T_2/T_1$), together with the intensity of the source ($q_0$), determine the level of pollution in the bottom and upper part of the canyon. In the case of a sinusoidal periodic source, the analysis revealed an increase in the amplitude of concentration oscillations as a function of the source period, as well as the damping of concentration peaks with vertical distance from street level. The introduction of stochastic noise to the emission was found to considerably enhance concentration fluctuations with respect to deterministic periodic behavior. This phenomenon is mainly attributed to the role of the tails of the *pdf* distribution at emission, capable of amplifying the non-linear effects of the system.

Simulations concerning reactive pollutants have brought attention to the non-linear relation between the mean concentrations in the two regions of the canyon, depending on the source intensity and the background $O_3$ concentration. Also, statistical analysis of concentration time series highlighted that the source period not only affects the second moment of the distribution but also its asymmetry, thereby influencing the occurrence of rare concentration peaks.

While the impact of street parameters on the mean air pollutant concentration is something that, although not extensively explored, aligns with previous studies, the stochastic analysis and the examination of higher-order statistics are innovative and provide crucial insights into extreme pollution levels which dramatically affect the exposure and, consequently, the health implications for citizens. Furthermore, the findings from this study can enhance the information provided by operational urban air quality models, e.g., SIRANE.

These results cover the standard deviation of concentration in street canyons, offering a more comprehensive understanding beyond temporal means, and reveal the spatial distribution of concentrations, through the application of multi-box models.

Despite the model being grounded in previously validated studies on both ventilation dynamics, experimental validation of the obtained results for inert gases through wind tunnel experiments would be desirable. On the other hand, validating the chemical aspects would require pollution measurements within an urban canyon and temporal trends in traffic flows.

The proposed methodology is highly adaptable and can be easily extended and refined. For instance, a natural progression of the work involves exploring various canyon geometries and wind directions. In both scenarios, ventilation times would be significantly influenced, and suitable multi-box models should be carefully implemented to represent recirculation zones within the canyon.

In addition, more comprehensive chemical models could be incorporated to account for the interaction of $NO_x$ with VOCs and hydrocarbons.Expanding the model's scope to simulate particulate matter dynamics is also feasible, requiring integration with sedimentation flow from the atmosphere above roofs and particle deposition to the ground.

Furthermore, this approach can be adapted to investigate the effect of various forcings exhibiting random components, such as atmospheric variability (different irradiation conditions, ventilation, or atmospheric stability), emissions (multiple sources within the canyon), or dynamics-related forcings (turbulence injection at street level due to vehicular traffic). Such scenario studies are crucial for assessing the impact of urban microclimate variations resulting from climate change on pollution levels and peak concentrations in the streets.

Finally, the model is particularly suitable for examining the effect of different strategies for regulating vehicular traffic, such as optimizing the cycle length of traffic signals.

## CRediT authorship contribution statement

**Sofia Fellini:** Writing – review & editing, Writing – original draft, Visualization, Validation, Software, Project administration, Methodology, Investigation, Formal analysis, Data curation, Conceptualization. **Pietro Salizzoni:** Writing – review & editing, Supervision, Project administration, Methodology, Investigation, Funding acquisition, Formal analysis. **Luca Ridolfi:** Writing – review & editing, Supervision, Methodology, Investigation, Funding acquisition, Formal analysis, Conceptualization.

## Declaration of competing interest

The authors declare that they have no known competing financial interests or personal relationships that could have appeared to influence the work reported in this paper.

## Data availability

Data will be made available on request.

## Appendix A. Vertical bulk exchange velocity in box models

The bulk exchange velocity between the upper part of the canyon and the external flow, $u_{1e}$, is defined (e.g., Fellini et al., 2020a) as the ratio between the vertical mass flux from the street cavity towards the external flow and the concentration difference $\langle C - C_e \rangle$:

$$u_{1e}(C - C_e)WL = \int_0^L \int_0^W [\langle wc \rangle]_{z=H} dydx, \tag{A.9}$$

where $W$, $L$ and $H$ are the width, length and height of the street canyon (in the direction $x$, $y$, and $z$ of the reference system), while $\langle wc \rangle$ is the ensemble mean of the total flux of pollutants in the vertical direction. Similarly, the velocity $u_{12}$ can be defined by considering the vertical mass flux between the two cells within the canyon and the difference in mean concentration between them.

## Appendix B. NO-$NO_2$-$O_3$ reaction cycle

The nitrogen cycle in the urban atmosphere involves numerous complex reactions. However, the main chemical transformations can be reliably reduced to the following scheme (e.g., Soulhac et al., 2011):

$$\begin{cases} NO_2 + h\nu \xrightarrow{k_1} NO + O^\bullet \\ O^\bullet + O_2 \xrightarrow{k_2} O_3 \\ NO + O_3 \xrightarrow{k_3} NO_2 + O_2, \end{cases} \tag{B.10}$$

where $NO_2$, NO and $O_3$ are nitrogen dioxides, nitrogen oxides and ozone, respectively, $O_2$ and $O^\bullet$ are oxygen and oxygen radicals, while $k_1$, $k_2$ and $k_3$ are kinetic constants of reaction. The reactivity of the radical $O^\bullet$ is so high that the second transformation is much faster than the first and the third ones (Seinfeld, 1986). The constants $k_1$ and $k_3$ are thus the limiting parameters of the cycle. The rate $k_1$ ($NO_2$ photolysis rate) mainly depends on the solar light intensity whereas $k_3$ mainly depends on the atmospheric temperature. These

dependences can be modelled by the following relations (Seinfeld, 1986; Soulhac et al., 2023):

$$\begin{cases} k_1 = \dfrac{1}{60}\left(0.5699 - \left[9.056 \cdot 10^{-3}(90-\chi)\right]^{2.546}\right)\left(1 - 0.75\left[\dfrac{\mathrm{Cld}}{8}\right]^{3.4}\right)(\mathrm{s}^{-1}) \\ k_3 = 1.325 \cdot 10^{6} exp\left(-\dfrac{1430}{\Theta}\right)(\mathrm{m}^3\mathrm{mol}^{-1}\mathrm{s}^{-1}), \end{cases} \tag{B.11}$$

where $\chi$ is the solar elevation (in degrees), *Cld* is the cloud coverage (in Okta) and Θ is temperature (in Kelvin). Thus, the production and destruction terms per unit volume for each chemical species can be related to the molar concentration by the following expressions:

$$p_{NO2} = k_3[NO][O_3], \qquad d_{NO} = k_1[NO_2] \tag{B.12}$$

$$p_{NO} = k_1[NO_2], \qquad d_{NO} = k_3[NO][O_3] \tag{B.13}$$

$$p_{O3} = k_1[NO_2], \qquad d_{O3} = k_3[NO][O_3], \tag{B.14}$$

where $[\cdot]$ represents the molar concentration (mol/m$^3$) of the compound.

## Appendix C. Coloured Gaussian noise

To mimic a realistic emission due to vehicular traffic, the source signal can be forced with a coloured Gaussian noise $X(t)$, which accounts for random fluctuations at the emission but maintains a characteristic temporal scale. The noise is obtained from the Ornstein-Uhlenbeck process and evolves over time according to:

$$\frac{dX(t)}{dt} = -\frac{1}{\tau}X(t) + \varepsilon^{1/2}\Gamma(t), \tag{C.15}$$

where $\tau$ and $\varepsilon$ are the relaxation time and the diffusion constant of the process, and $\Gamma(t)$ is a Gaussian white noise. The diffusion constant amplifies the noise, while the relaxation time is representative of the autocorrelation of the signal, that mimics the periodicity of vehicle transits. For $\tau \to 0$ the signal tends to a Gaussian white noise, i.e. a completely uncorrelated noise. The coloured noise is added to the mean emission $q_0$, so that:

$$q(t) = q_0 + X(t). \tag{C.16}$$

According to Gillespie (1996), the exact updating formula for $X$ at each time increment $\Delta t$ in a numerical simulation is:

$$X(t+\Delta t) = X(t)\mu + \sigma n \tag{C.17}$$

where $n$ are statistically independent unit random numbers and

$$\mu = e^{-\Delta t/\tau}, \tag{C.18}$$

$$\sigma^2 = (\varepsilon\tau/2)\left(1-\mu^2\right). \tag{C.19}$$

After a sufficiently long time ($t \gg \tau$), the mean and variance of $X(t)$ are 0 and $\varepsilon\tau/2$, respectively. As a consequence, the mean and variance of $q$ (see Eq. C.16) are $q_0$ and $\varepsilon\tau/2$.

## Appendix D. Probability density functions of concentration for a sinusoidal source with long period

For $\tau/T_1 \to \infty$, the ventilation process is much faster than the emission timescale, $\varepsilon$ approaches zero (Eq. 7), and the emission noise varies so slowly that the system behaves like a succession of stationary states. As a consequence, the relation between emission and concentration is independent on time and follows the same relations found in Eqs. 8 for the solution with steady emission. In this case, the *pdf* of the concentrations can be analytically found as derived distribution of the source *pdf*:

$$p(C_1, \tau\to\infty) = p(q)\frac{dq}{dC_1} = \tag{D.20}$$

$$= \frac{1}{\alpha T_1\sqrt{\pi\varepsilon\tau}} exp\left[-\frac{\left(\frac{C_1}{\alpha T_1} - q_0\right)^2}{\varepsilon\tau}\right] \tag{D.21}$$

$$p(C_2, \tau\to\infty) = p(q)\frac{dq}{dC_2} = \tag{D.22}$$

$$= \frac{1}{(\alpha T_1 + T_2)\sqrt{\pi\varepsilon\tau}} exp\left[ -\frac{\left(\frac{C_1}{\alpha T_1 + T_2} - q_0\right)^2}{\varepsilon\tau} \right]. \quad (D.23)$$

As mentioned above, these distributions are valid only for $\tau/T_1 \to \infty$ and are reported in Fig. 5.b-c as dotted grey line. The distributions for the concentration are again Gaussian distributions, as for the emission. For $C_1$, the variance is $\frac{\varepsilon\tau}{2}\alpha^2 T_1^2$ and the mean is $\alpha T_1 q_0$. For $C_2$, the variance is $\frac{\varepsilon\tau}{2}(\alpha T_1 + T_2)^2$ and the mean is $(\alpha T_1 + T_2)q_0$. Thus the coefficient of variation in both cases is $\sqrt{\frac{\varepsilon\tau}{2}}\ \frac{1}{q_0}$, i.e. the same as the source distribution. This confirms the results found in Fig. 3.c for $\tau/T_1 \to \infty$.

## Appendix E. Supplementary data

Supplementary data to this article can be found online at https://doi.org/10.1016/j.uclim.2024.101952.

## References


Allegrini, J., Dorer, V., Carmeliet, J., 2013. Wind tunnel measurements of buoyant flows in street canyons. Build. Environ. 59, 315–326.

Anenberg, S.C., Mohegh, A., Goldberg, D.L., Kerr, G.H., Brauer, M., Burkart, K., Hystad, P., Larkin, A., Wozniak, S., Lamsal, L., 2022. Long-term trends in urban NO2 concentrations and associated paediatric asthma incidence: estimates from global datasets. The Lancet Planetary Health 6 (1), e49–e58.

Assimakopoulos, V.D., ApSimon, H., Moussiopoulos, N., 2003. A numerical study of atmospheric pollutant dispersion in different two-dimensional street canyon configurations. Atmos. Environ. 37 (29), 4037–4049.

Berkowicz, R., 2000. OSPM-A parameterised street pollution model. Environ. Monit. Assess. 65 (1–2), 323–331.

Bloomberg, L., Dale, J., 2000. Comparison of vissim and corsim traffic simulation models on a congested network. Transp. Res. Rec. 1727 (1), 52–60.

Bright, V.B., Bloss, W.J., Cai, X., 2013. Urban street canyons: coupling dynamics, chemistry and within-canyon chemical processing of emissions. Atmos. Environ. 68, 127–142.

Carlo, O.S., Fellini, S., Palusci, O., Marro, M., Salizzoni, P., Buccolieri, R., 2023. Influence of obstacles on urban canyon ventilation and air pollutant concentration: an experimental assessment. Build. Environ. 111143.

Carruthers, D., Edmunds, H., Lester, A., McHugh, C., Singles, R., 2000. Use and validation of ADMS-urban in contrasting urban and industrial locations. Int. J. Environ. Pollut. 14 (1–6), 364–374.

Carslaw, D.C., Murrells, T.P., Andersson, J., Keenan, M., 2016. Have vehicle emissions of primary NO2 peaked? Faraday Discuss. 189, 439–454.

Cassiani, M., Bertagni, M.B., Marro, M., Salizzoni, P., 2020. Concentration fluctuations from localized atmospheric releases. Bound.-Layer Meteorol. 1–50.

Caton, F., Britter, R., Dalziel, S., 2003. Dispersion mechanisms in a street canyon. Atmos. Environ. 37 (5), 693–702.

Del Ponte, A.V., Fellini, S., Marro, M., van Reeuwijk, M., Ridolfi, L., Salizzoni, P., 2024. Influence of street trees on turbulent fluctuations and transport processes in an urban canyon: a wind tunnel study. Bound.-Layer Meteorol. 190 (2).

EEA, 2021. Managing Air Quality in Europe. Briefing no, p. 19/2021.

Fellini, S., Ridolfi, L., Salizzoni, P., 2020a. Street Canyon Ventilation: Combined Effect of Cross-Section Geometry and Wall Heating. Q. J. R. Meteorol. Soc.

Fellini, S., Salizzoni, P., Ridolfi, L., 2020b. Centrality metric for the vulnerability of urban networks to toxic releases. Phys. Rev. E 101 (3), 032312.

Fellini, S., Salizzoni, P., Ridolfi, L., 2021. Vulnerability of cities to toxic airborne releases is written in their topology. Sci. Rep. 11 (1), 23029.

Fellini, S., Marro, M., Del Ponte, A.V., Barulli, M., Soulhac, L., Ridolfi, L., Salizzoni, P., 2022. High resolution wind-tunnel investigation about the effect of street trees on pollutant concentration and street canyon ventilation. Build. Environ. 226, 109763.

Garmory, A., Kim, I., Britter, R., Mastorakos, E., 2009. Simulations of the dispersion of reactive pollutants in a street canyon, considering different chemical mechanisms and micromixing. Atmos. Environ. 43 (31), 4670–4680.

Gillespie, D.T., 1996. Exact numerical simulation of the ornstein-uhlenbeck process and its integral. Phys. Rev. E 54 (2), 2084.

Gromke, C., Ruck, B., 2012. Pollutant concentrations in street canyons of different aspect ratio with avenues of trees for various wind directions. Bound.-Layer Meteorol. 144 (1), 41–64.

Grylls, T., Le Cornec, C.M., Salizzoni, P., Soulhac, L., Stettler, M.E., Van Reeuwijk, M., 2019. Evaluation of an operational air quality model using large-eddy simulation. Atmospheric Environment: X 3, 100041.

Jenkin, M.E., Clemitshaw, K.C., 2000. Ozone and other secondary photochemical pollutants: chemical processes governing their formation in the planetary boundary layer. Atmos. Environ. 34 (16), 2499–2527.

Jeong, S.J., Andrews, M.J., 2002. Application of the k–$\varepsilon$ turbulence model to the high Reynolds number skimming flow field of an urban street canyon. Atmos. Environ. 36 (7), 1137–1145.

Khreis, H., Kelly, C., Tate, J., Parslow, R., Lucas, K., Nieuwenhuijsen, M., 2017. Exposure to traffic-related air pollution and risk of development of childhood asthma: a systematic review and meta-analysis. Environ. Int. 100, 1–31.

Kim, M.J., Park, R.J., Kim, J.-J., 2012. Urban air quality modeling with full O3-NOx-VOC chemistry: implications for O3 and PM air quality in a street canyon. Atmos. Environ. 47, 330–340.

Kovar-Panskus, A., Louka, P., Sini, J.-F., Savory, E., Czech, M., Abdelqari, A., Mestayer, P., Toy, N., 2002. Influence of geometry on the mean flow within urban street canyons–a comparison of wind tunnel experiments and numerical simulations. Water, Air and Soil Pollution: Focus 2 (5–6), 365–380.

Kukkonen, J., Valkonen, E., Walden, J., Koskentalo, T., Aarnio, P., Karppinen, A., Berkowicz, R., Kartastenpää, R., 2001. A measurement campaign in a street canyon in Helsinki and comparison of results with predictions of the OSPM model. Atmos. Environ. 35 (2), 231–243.

Kwak, K.-H., Baik, J.-J., 2012. A CFD modeling study of the impacts of NOx and VOC emissions on reactive pollutant dispersion in and above a street canyon. Atmos. Environ. 46, 71–80.

Lee, I.Y., Park, H.M., 1994. Parameterization of the Pollutant Transport and Dispersion in Urban Street Canyons, 28, pp. 2343–2349, 14.

Li, Z., Ming, T., Liu, S., Peng, C., de Richter, R., Li, W., Zhang, H., Wen, C.-Y., 2021. Review on pollutant dispersion in urban areas-part a: effects of mechanical factors and urban morphology. Build. Environ. 190, 107534.

Li, T., Fellini, S., van Reeuwijk, M., 2023. Urban air quality: what is the optimal place to reduce transport emissions? Atmos. Environ. 292, 119432.

Liu, C.-H., Leung, D.Y., 2008. Numerical study on the ozone formation inside street canyons using a chemistry box model. J. Environ. Sci. 20 (7), 832–837.

Liu, C.-H., Barth, M.C., Leung, D.Y., 2004. Large-eddy simulation of flow and pollutant transport in street canyons of different building-height-to-street-width ratios. J. Appl. Meteorol. 43 (10), 1410–1424.

Louka, P., Vachon, G., Sini, J.-F., Mestayer, P., Rosant, J.-M., 2002. Thermal effects on the airflow in a street canyon - Nantes' 99 experimental results and model simulations. Water, Air and Soil Pollution: Focus 2 (5–6), 351–364.

Marucci, D., Carpentieri, M., 2019. Effect of local and upwind stratification on flow and dispersion inside and above a bi-dimensional street canyon. Build. Environ. 156, 74–88.
Murena, F., Di Benedetto, A., D'Onofrio, M., Vitiello, G., 2011. Mass transfer velocity and momentum vertical exchange in simulated deep street canyons. Bound.-Layer Meteorol. 140 (1), 125.
Murray, C.J., Aravkin, A.Y., Zheng, P., Abbafati, C., Abbas, K.M., Abbasi-Kangevari, M., Abd-Allah, F., Abdelalim, A., Abdollahi, M., Abdollahpour, I., et al., 2020. Global burden of 87 risk factors in 204 countries and territories, 1990–2019: a systematic analysis for the global burden of disease study 2019. Lancet 396 (10258), 1223–1249.
Ntziachristos, L., Samaras, Z., Eggleston, S., Gorissen, N., Hassel, D., Hickman, A., et al., 2000. Copert iii. Computer Programme to calculate emissions from road transport, methodology and emission factors (version 2.1). European Energy Agency (EEA), Copenhagen.
Oke, T.R., Mills, G., Christen, A., Voogt, J.A., 2017. Urban climates. Cambridge University Press.
Panis, L.I., Broekx, S., Liu, R., 2006. Modelling instantaneous traffic emission and the influence of traffic speed limits. Sci. Total Environ. 371 (1–3), 270–285.
Salizzoni, P., 2006. Mass and Momentum Transfer in the Urban Boundary Layer. PhD thesis,. Ecully, Ecole centrale de Lyon.
Salizzoni, P., Soulhac, L., Mejean, P., 2009. Street canyon ventilation and atmospheric turbulence. Atmos. Environ. 43 (32), 5056–5067.
Seinfeld, J.H., 1986. Atmospheric Chemistry and Physics of Air Polution. California Institute of Technology Pasadena, California.
Sini, J.-F., Anquetin, S., Mestayer, P.G., 1996. Pollutant dispersion and thermal effects in urban street canyons. Atmos. Environ. 30 (15), 2659–2677.
Soulhac, L., 2000. Modélisation de la dispersion atmosphérique à l'intérieur de la canopée urbaine. PhD thesis,. Ecole Centrale de Lyon.
Soulhac, L., Salizzoni, P., 2010. Dispersion in a street canyon for a wind direction parallel to the street axis. J. Wind Eng. Ind. Aerodyn. 98 (12), 903–910.
Soulhac, L., Perkins, R.J., Salizzoni, P., 2008. Flow in a street canyon for any external wind direction. Bound.-Layer Meteorol. 126 (3), 365–388.
Soulhac, L., Salizzoni, P., Cierco, F.-X., Perkins, R., 2011. The model SIRANE for atmospheric urban pollutant dispersion; part I, presentation of the model. Atmos. Environ. 45 (39), 7379–7395.
Soulhac, L., Salizzoni, P., Mejean, P., Didier, D., Rios, I., 2012. The model sirane for atmospheric urban pollutant dispersion; part ii, validation of the model on a real case study. Atmos. Environ. 49, 320–337.
Soulhac, L., Fellini, S., Nguyen, C.V., Salizzoni, P., 2023. Evaluation of Photostationary and Non-photostationary Operational Models for nox Pollution in a Street Canyon. Atmospheric Environment, p. 119589.
Vardoulakis, S., Valiantis, M., Milner, J., ApSimon, H., 2007. Operational air pollution modelling in the UK — street canyon applications and challenges. Atmos. Environ. 41 (22), 4622–4637.
WHO, 2023. WHO Ambient Air Quality Database (update 2023). version 6.0.
Xiaomin, X., Zhen, H., Jiasong, W., 2006. The impact of urban street layout on local atmospheric environment. Build. Environ. 41 (10), 1352–1363.
Zhong, J., Cai, X.-M., Bloss, W.J., 2015. Modelling the dispersion and transport of reactive pollutants in a deep urban street canyon: using large-eddy simulation. Environ. Pollut. 200, 42–52.
Zhong, J., Cai, X.-M., Bloss, W.J., 2016a. Coupling dynamics and chemistry in the air pollution modelling of street canyons: a review. Environ. Pollut. 214, 690–704.
Zhong, J., Cai, X.-M., Bloss, W.J., 2016b. Modelling photochemical pollutants in a deep urban street canyon: application of a coupled two-box model approximation. Atmos. Environ. 143, 86–107.